Accelerated lifetime metrology of EUV multilayer mirrors in hydrocarbon environments

S. B. Hill[*a], N. S. Faradzhev[a], C. Tarrio[a], T. B. Lucatorto[a],
T. E. Madey[b], B. V. Yakshinskiy[b], E. Loginova[†b] , S. Yulin[c]

[a]NIST, 100 Bureau Drive, Stop 8411, Gaithersburg, MD 20853-8411
[b]Rutgers University, Department of Physics and Astronomy, Piscataway, NJ 08854-8019
[c]Fraunhofer-Institut für Angewandte Optik und Feinmechnik, Jena, Germany

ABSTRACT

The ability to predict the rate of reflectivity loss of capped multilayer mirrors (MLMs) under various conditions of ambient vacuum composition, intensity, and previous dose is crucial to solving the mirror lifetime problem in an EUV stepper. Previous measurements at NIST have shown that reflectivity loss of MLMs exposed under accelerated conditions of dose and pressure can be a very complicated function of these variables. The present work continues this effort and demonstrates that reflectivity loss does not scale linearly for accelerated exposure doses over the range of 0-350 J/mm^2 either for partial pressures of MMA in the range 10^{-8}-10^{-7} Torr or acetone in the range 10^{-7}-10^{-6} Torr. We suggest that this nonlinear scaling may be the result of a varying damage rate as the surface of the growing contamination layer moves through the EUV standing wave created by exposure of any MLM to resonant radiation. To further investigate the potential influence of these resonance effects, we report new measurements showing large variations of the secondary electron yield as a function of thickness of carbon deposited on top of a MLM.

Keywords: extreme ultraviolet; lithography; reflectometry; EUV optics; ruthenium films; lifetime testing

1. INTRODUCTION

The commercialization of EUV lithography high volume manufacturing will require the multilayer mirrors (MLMs) in the projection box of a stepper to have a lifetime of 30,000 hours without a decrease in reflectivity of more than a few percent.[1,2] Recent experience in several laboratories with micro exposure tools (METs) (prototype steppers) has shown that carbonization is the major source of reflectivity loss, and that loss of over a few percent occurs in times only a small fraction of the required 30,000 hours. The carbonization is caused by the photon-induced cracking of the residual hydrocarbons in the ambient vacuum of the stepper coming from resist outgassing and other sources. During the last year NIST has continued its lifetime testing studies with a focus on carbon growth and on improved analysis of the surface changes that accompany the loss in reflectivity.

2. MULTILAYER LIFETIME TESTING

2.1. EUV exposure facility at NIST

The facility installed on SURF-III and illustrated in Figure 1 was designed to maximize throughput and minimize contamination associated with sample introduction. The chamber has a smooth electropolished finish, and most of the components exposed to vacuum are plated with a 0.5μm layer of gold to minimize adsorption of water, diffusion of hydrogen through the stainless steel and desorption of contaminant species from the chamber walls. The exposure chamber is bakeable to 150ºC, limited only by the photodiodes used to measure the intensity of the incident and reflected

[*] shill@email.nist.gov; phone (301) 975 4283; fax (301) 926 2746; nist.gov
[†] Present affiliation is Sandia National Laboratories, Livermore, CA 94550

EUV radiation. Samples are introduced through a gold-plated loadlock. All pumps are completely oil free. The base pressure in the chamber is routinely in the mid 10^{-11} Torr range.

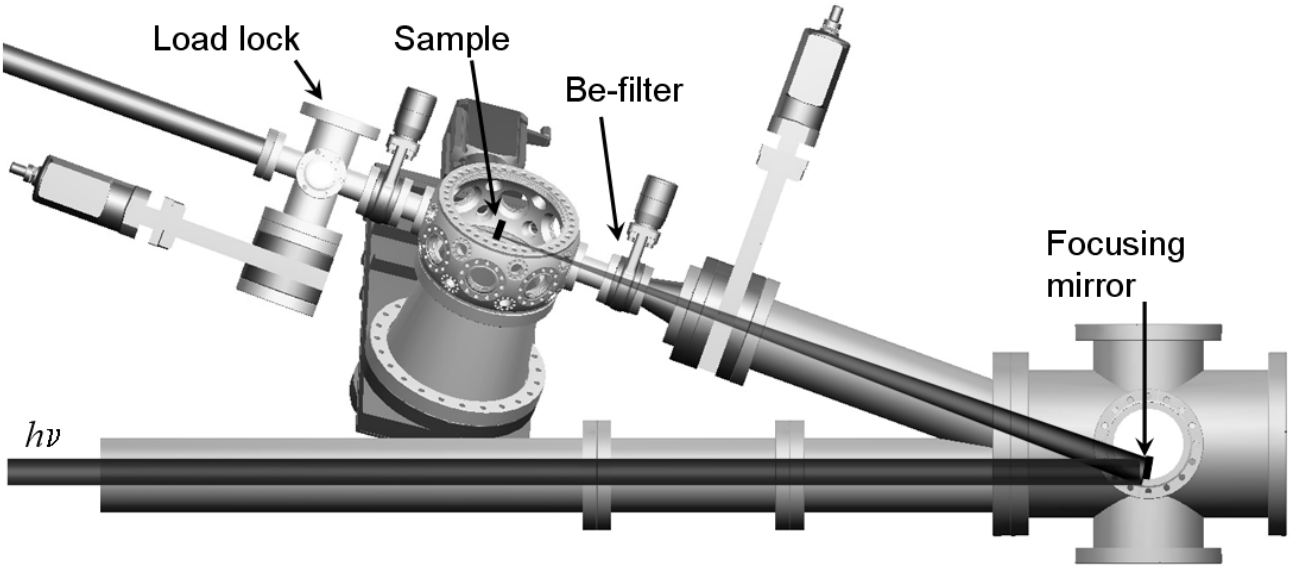

Fig.. 1. Schematic of the end-station on the SURF III synchrotron for endurance testing of EUV optics at NIST

The output of the synchrotron is collected by a near-normal-incident ML mirror placed approximately 4 m from the storage ring tangent point. This MLM is designed to reflect EUV radiation with a 6-degree angle of incidence in the bandwidth 13.1 nm to 13.6 nm with approximately 50% efficiency. Due to pre-existing geometry, however, mirrors are exposed at 10º in our chamber. A 200 nm-thick beryllium filter completely blocks long-wavelength light while transmitting 50-60% of the EUV radiation. More importantly, this filter also serves as a physical barrier separating the exposure chamber from the rest of the beamline. It is essential that the synchrotron and the focusing mirror not be exposed to the high levels of water and/or hydrocarbon vapors present in the exposure chamber. The transmission of the exposure beam is checked periodically by a calibrated photodiode.

The MLM under test is placed near the focal spot of the EUV beam and oriented to reflect the incident radiation at 10 degrees. The focal spot has an asymmetric Gaussian intensity distribution and full widths at half maxima (FWHM) of 1.0 mm and 0.5 mm. The peak intensity follows the synchrotron beam decay cycle and decreases smoothly from (7.5 to 3.8)±0.3 mW/mm^2 over the course of 4-5 hours before a new beam is injected. In our experiments, the accumulation of high exposure doses requires several injections (e.g. 200 J/mm^2 requires 2.5 decay-injection cycles). Two Mo-Si coated photodiodes are used to make *in situ* reflectivity measurements. These *in situ* measurements, however, lack the precision to measure accurately the critical 1-2% changes in reflectivity at 13.5 nm and do not provide any information on the spatial distribution of the damage. High spatial-resolution post-exposure reflectometry is performed at the Lawrence Berkeley National Lab's Advanced Light Source to measure precisely the reflectivity at 13.5 nm in 100 μm steps over the entire exposure spot. (Although the 0.3% absolute uncertainty of the reflectometer at NIST is certainly sufficient for this task, the Berkeley facility provides better spatial resolution.)

In order to accelerate the reflectivity loss due to various species that might be encountered in a stepper during testing, the partial pressure of a selected species can be varied between the base pressure of $<1\times10^{-9}$ Torr and 5×10^{-6} Torr, which is considerably greater than the expected base pressure in the PO box. Here, we report mainly on our studies of two hydrocarbon molecules, MMA and acetone, but we have also studied exposures in water vapor, CO, CO_2, H_2, methanol, benzene and toluene. The average intensity at the test sample is at least 10 times the maximum intensity predicted on most projection optics in a commercial stepper and might be comparable with the intensity expected for illumination optics. This allows limited scaling studies to investigate the dependence of damage rate on various adjustable quantities that could be used to accelerate the lifetime tests.

3. CHARACTERIZATION OF PHOTON-INDUCED SURFACE CHANGES

The two primary mechanisms responsible for photon-induced reflectivity loss of a MLM are C-deposition from cracked hydrocarbons and oxidation by ambient water vapor. In general, to determine the exact nature of the change to the surface one needs to involve techniques sensitive to the elemental and chemical composition of the surface (e.g. XPS, AES, TOF-SIMS) and its structure and morphology (e.g. SEM, AFM, etc). Since these techniques can be expensive, time consuming and of limited availability, it is important to know when a detailed understanding of the damage is required and when a simple reflectivity measurement will suffice to quantify the damage from a given exposure.

In this paper we will focus on exposures in hydrocarbon-dominated environments in which case the primary source of reflectivity decay is simple deposition of C on the mirror surface. The exact morphology and composition of the carbonaceous layer may vary slightly for different hydrocarbons, but it should be similar for exposures in different pressures of the same hydrocarbon. This would suggest that reflectometry alone could be used to compare the damage done by exposing a MLM to different EUV doses and pressures of the same gas. Even in this simple case, however, additional surface analysis may be required since the reflectivity of a MLM does not always decrease monotonically with the thickness of deposited C. In this section we discuss examples of both experimental data and simulated reflectivity calculations that demonstrate the conditions under which reflectometry alone is sufficient to quantify the degree of damage. We also discuss a case involving exposure of Ru-capped MLM to H_2O in which the reflectivity data was ambiguous until correlated with XPS analysis.

3.1. Reflectometry

After a sample is exposed in the NIST testing facility, high-spatial-resolution reflectometry is performed at the Advanced Light Source (ALS) at the Lawrence Berkeley Laboratory which determines the reflectivity at 100 μm intervals along a line through the center of the exposure spot. Since the intensity distribution of the EUV beam is well characterized, each point in the reflectivity profile can be correlated to the dose at that location. So a single exposure in our facility yields information over a wide range dose response.

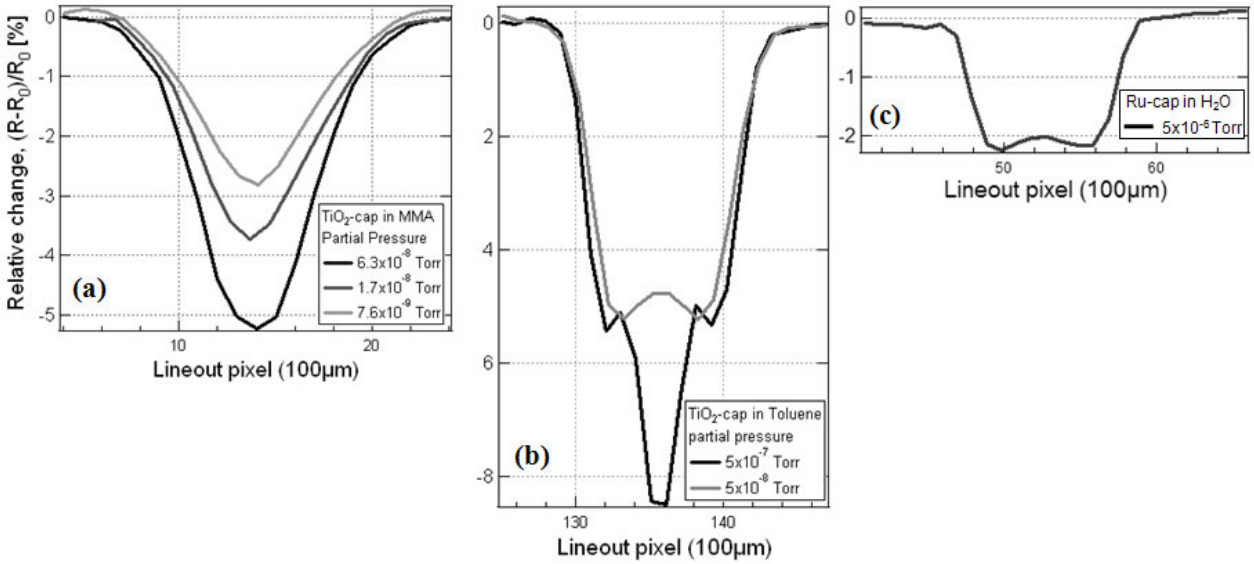

Fig. 2 Diversity of reflectivity profiles detected after various EUV light doses on different MLMs {(a,b) TiO_2-capped MLM, (c) Ru-capped MLM} with different ambient gasses introduced {(a) MMA, (b) toluene, (c) water}

Figure 2 shows examples of reflectivity profiles resulting from different exposures on different MLMs. Although the EUV exposure beam has a Gaussian spatial distribution, the reflectivity profiles sometimes have a distinctly non-Gaussian shape. This, however, does not necessarily imply that the changes in the MLM surface have a non-Gaussian spatial profile. Due to the inherently resonant nature of MLMs, the reflectivity does not decrease monotonically with

increasing C thickness on the mirror surface. Figure 3(a) shows an example of how the reflectivity of a typical MLM structure changes as a function of deposited C thickness. The thicknesses at which the local maxima and minima occur as well as the overall slope of the curve are assumed to depend on the exact structure of the MLM and capping layer, the wavelength and angle of incidence of the light, and the density of the deposited C. Since our studies have encompassed different MLMs with different cap layers, it is critically important to include this nonlinear relationship between reflectivity and C thickness when interpreting the reflectometry of our exposures.

Since our exposure beam has a Gaussian spatial profile, one might expect a Gaussian distribution of C thicknesses across a given exposure spot. Figure 3(b) shows the calculated reflectivity profiles that would result from the same Gaussian spatial distribution of C on different hypothetical MLMs with different overall phases (i.e., location of the z=0 point) of of the R-vs.-C-thickness curve shown in Figure 3(a). It seems clear that the "bump" in the reflectivity profiles for the toluene ($C_6H_5CH_3$) exposure shown in Figure 2 is the result of a native MLM structure and distribution of C thicknesses that includes one of the peaks in the R-vs.-C-thickness curve as in case III of Figure 3. The MMA (methyl methacrylate, $C_5H_8O_2$) exposures of different MLMs shown in Figure 2, however, appear to produce C thicknesses that remain entirely in the linear regime between reflectivity maxima as in case II of Figure 3. Only in this latter case can one assume a direct linear relationship between the reflectivity loss and C thickness. We will show that all of the hydrocarbon exposures discussed in Sec. 4 below fall into this category.

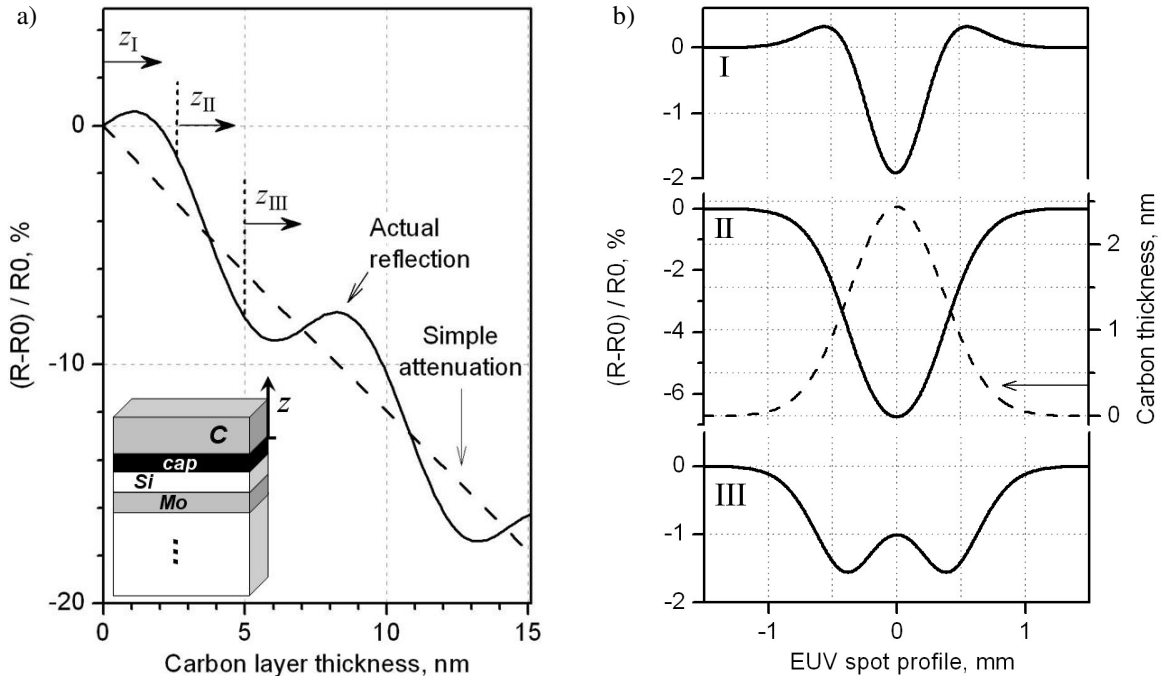

Fig. 3 (a) Plot showing resonant oscillations in the reflectivity of a multilayer mirror (solid line) as a function of increasing thickness of carbon overlayer. For reference, the dash line demonstrates simple attenuation of the EUV light that would be absorbed by a thin carbon film. (b) Calculated reflectivity profiles (solid lines) of MLMs with the same Gaussian spatial distribution of deposited carbon (dash line). Different curves (labels I, II and III) correspond to different hypothetical MLMs with different locations of the native cap/vacuum interface (z=0) as marked in plot (a).

3.2. Surface analysis using XPS

Reflectometry profiles with a non-Gaussian shape must be further analyzed to determine whether the shape is due to the measurement resonances discussed above or to a truly non-Gaussian distribution of EUV-induced change to the surface. The water exposure shown in Figure 2 is an example of a non-Gaussian reflectivity profile that corresponds to a non-Gaussian damage profile. We analyzed damage profile using X-ray photoelectron spectroscopy (XPS) which allowed us to determine variation of elemental and chemical composition across EUV exposed area of the surface. In our

experiments the source was operating at 140W. The spectra are recorded at normal take off angle using small spot regime with 110 μm aperture and pass energies 160 eV for surveys and 20 eV for high resolution spectra. The surface of the sample is mapped with 100 μm step in the vicinity of EUV exposed areas. The chemical state information is extracted by fitting of high resolution XPS spectra using CasaXPS software (release 2.3.12).

The component analysis of the spectra in $Ru3d_{5/2}$ region indicates excess of the oxidized ruthenium in the area where intense EUV light hits the surface. The symbols in Figure 4 plot the variation of metallic (filled circles) and oxidic (open circles) ruthenium component integrals across the EUV spot. In contrast to Gaussian profile of EUV beam (dash line), the distribution of oxidic ruthenium across the spot exhibits saturation in the highest light intensity area. The similar trend is observed in O1s region (not shown here). Simultaneously, the drop of metallic ruthenium signal demonstrates the flat bottom profile. This variation of ruthenium chemical state is obviously non-Gaussian and looks very similar to reflection profile (solid line).

An explanation consistent with the data of Figure 4 is a site-limited oxidation of ruthenium film where the first, very rapid oxidation of the cap induced by EUV light in the presence of water happens at defect sites (e.g. grain boundaries, steps, etc). After "filling in" all such sites, the oxidation may proceed further into the bulk of the ruthenium microcrystallites with much slower rate. This would lead to a saturation effect of oxidation of top layer resulting in saturation of mirror reflectivity losses in the area of the dense photon flux. The chemistry of water on Ru induced by EUV and low energy electrons is discussed in detail elsewhere [3,4].

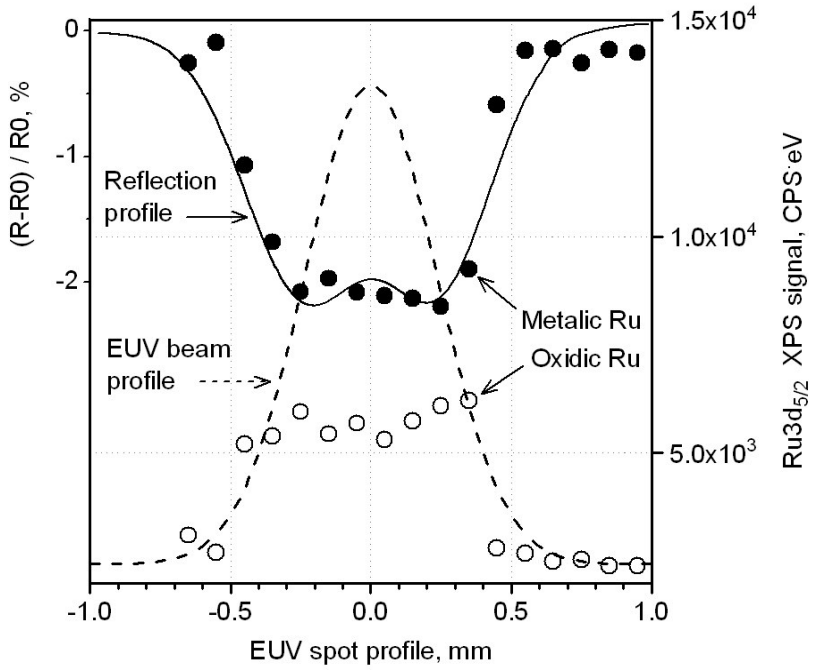

Fig. 2 Comparison of EUV beam profile (dash line), reflection loss profile (solid line) of the EUV exposed area of Ru coated MLM, and the surface analysis data (circles). The exposure is done at water atmosphere (partial pressure 5×10^{-6} Torr). Reflection is measured with the small beam size at Advanced Light Source (ALS), Berkeley, CA. The surface analysis is performed at NIST, Gaithersburg, MD using commercial X-ray photoelectron spectrometer Kratos Axis Ultra (monochromatized Al K_α radiation; base pressure is 5×10^{-10} Torr) operating in a small spot analysis mode. The variation of metallic (filled circles) and oxidized (open circles) ruthenium component integrals in $Ru3d_{5/2}$ region is plotted as function the surface distance across exposure spot with 100 μm step.

4. METHYL METHACRYLATE AND ACETONE EXPOSURES

To investigate how the damage to MLMs is accelerated as a function of pressure and dose, a series of exposures of TiO_2-capped MLMs were carried out over a range of pressures of MMA and acetone. It should be pointed out that this

particular TiO_2 capping formulation was not in any way optimized to resist C-deposition. Figure 2 shows a sampling of the reflectivity profiles of exposures spanning the range of MMA pressures used. As discussed above, the fact that all profiles mimic the Gaussian distribution of the exposure beam indicates that it is safe to assume that these exposures occurred in the linear regime of the R-vs-C-thickness curve where the reflectivity loss is directly proportional to the thickness of the deposited C layer. The reflectivity profiles for the acetone exposures also appeared to be in this linear regime.

4.1. Pressure dependence

Figure 5 shows the relative reflectivity drop as a function of pressure for different doses of the MMA and acetone exposures. The most obvious feature of the data is that the damage appears to saturate at pressures above some critical value for all doses. This type of behavior can be understood by considering that the damage rate must be proportional to the surface coverage of the hydrocarbon molecules as they are cracked by the EUV or resulting secondary electrons. For pressures well below the vapor pressure of the molecule at room temperature, this coverage will be limited to a monolayer (ML) or less (~10^{15} molecules cm^{-2}). So as the pressure is increased, eventually the coverage, and hence the damage rate, saturates, so that further increases in pressure will not result in greater coverage or damage. The solid lines in Figure 5 are the results of a simple model of C deposition based on Langmuir adsorption and a coverage which saturates at 1ML. While the model shows excellent qualitative agreement with the data, it is too crude to make quantitative predictions. An extended discussion of this model will be the subject of a forthcoming publication.

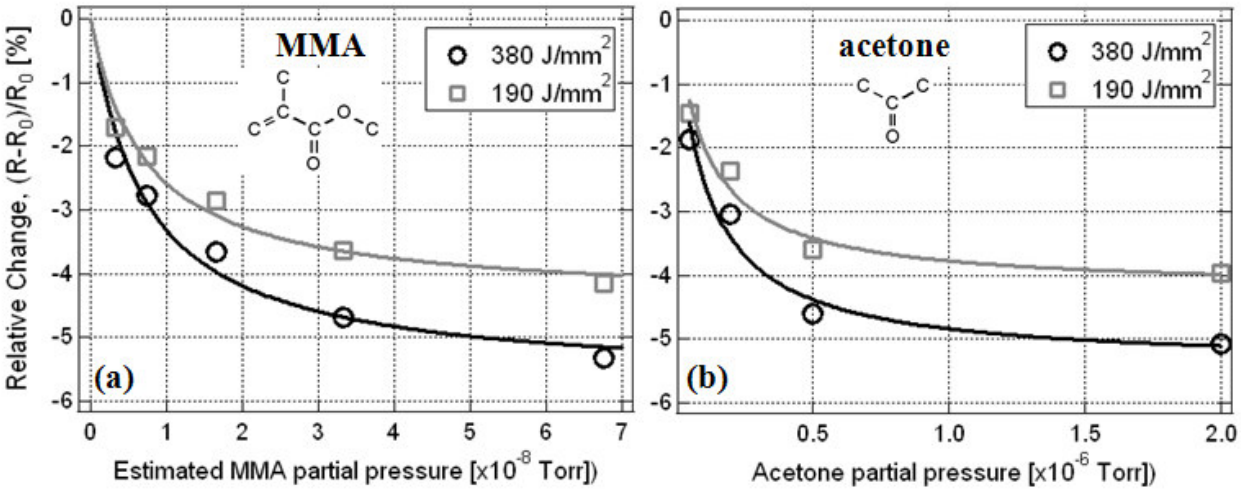

Fig. 5 Relative reflectivity changes of TiO_2-terminated MLM as a function of pressure of two hydrocarbon molecules: MMA (a) and Acetone (b). Data are shown for different EUV light doses. Due to uncertainties in the ionization probability for MMA, the absolute partial pressure of MMA could be up to twice the values reported here.

The nonlinear variation of damage with pressure has important implications for scaling the results of accelerated endurance testing. Since increasing pressure does not always result in increasing damage, the results of a low-dose, high-pressure exposure should not be scaled to predict the results of a higher-dose, low-pressure exposure without first determining whether the pressures used are in the linear regime or the saturation regime.

4.2. Dose dependence

While the pressure dependence of the MMA and acetone exposures is qualitatively explained by the concept of saturation coverage, the dose dependence is not. Note that the reflectivity losses for the 190 J/mm^2 curves in Figure 5 are not half those for the 390 J/mm^2 curves. This nonlinearity is more clearly seen in Figure 6 which shows the relative reflectivity drop for a few of the MMA exposures as a function of dose. It would appear that the damage rate is different at low and high doses. The slopes of the curves are steepest at low doses indicating that the deposition rate slows as C builds up. Such a change would be expected during the first ~1 nm of growth or ~1% of relative reflectivity loss since the SEY for C is smaller than that for the native TiO_2. Due to the sub-2-nm escape depth of low energy secondary

electrons, however, this transition should be complete after the first nanometer or two, yet the damage rate continue to slow over the entire range of reflectivity loss. Without knowing exactly how the relative reflectivity loss varies with dose, it is impossible to accurately predict the low-dose damage rates from these types of high-dose tests. Since this is the goal of accelerated testing, this nonlinearity must be understood.

One possible explanation would be that the damage rate actually has a nonlinear intensity dependence. Recall that the dose response for each pressure shown in Figure 6 was determined from a single spot exposed for a fixed time to the distribution of intensities defined by the Gaussian exposure beam. However, preliminary tests of Ru-capped MLM exposed in 5×10^{-8} Torr of toluene to equal EUV doses but intensities that differed by ~50% revealed essentially identical damage profiles when examined by XPS.

Another possibility could be that the rate remains constant but the density or composition of the contamination layer changes with dose. For example, it is found that C deposited on TiO_2 single crystal forms islands for the first nanometers of growth before the surface is completely covered [5] We also do not exclude that the amount of O incorporated into the contaminant layer is continuously reduced by photon stimulated desorption. Since O is much more absorbing than C in the EUV, this could lead to an apparent decrease in rate of reflectivity loss at higher doses.

As discussed in Sec. 3, only more detailed surface analysis could determine whether these potential effects could be playing a significant role. Based on secondary electron measurements discussed in the next section, the most likely explanation for the apparent change of damage rate is the known variation of the local EUV intensity and SEY as the surface grows through the resonant standing wave created by the MLM.

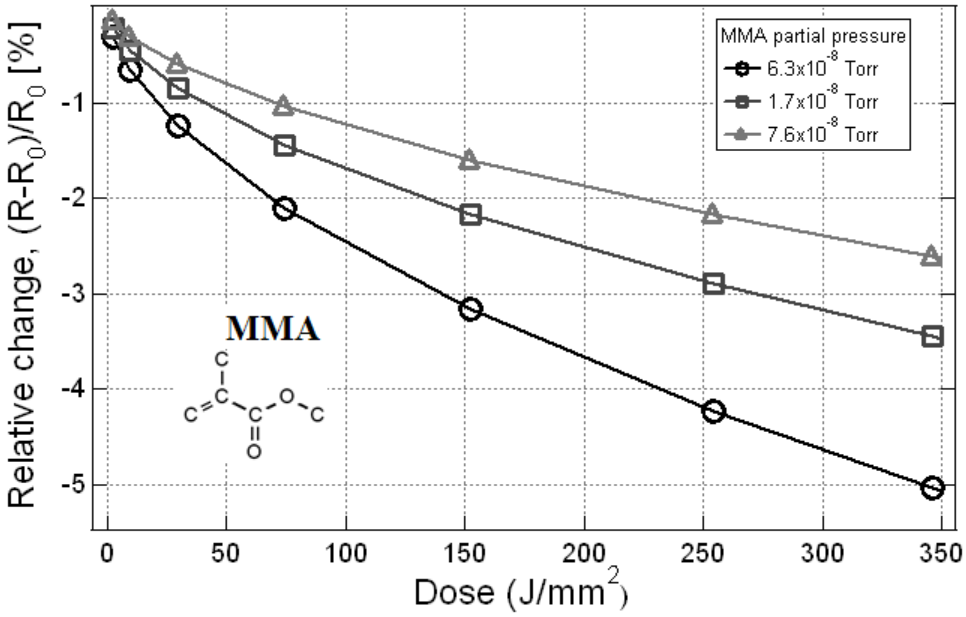

Fig. 6 Relative reflectivity changes of TiO_2-terminated MLM as a function of EUV light dose. The exposures are done at different partial pressures of MMA. Due to uncertainties in the ionization probability for MMA, the absolute partial pressure of MMA could be up to twice the reported values.

5. OBSERVATIONS AND IMPLICATIONS OF SEY RESONANCES

Just as the resonant structure of the MLM be considered when interpreting the reflectometry of exposed samples as discussed in Sec. 3, it can significantly influence the rate of damage as well. The constructive interference responsible for the high reflectivity of MLMs produces a standing wave of intensity that extends into the vacuum. As illustrated in Figure 7, for a typical reflectivity of 67%, the local value of the intensity can range from nearly zero to ~3.3 times the measured incidence intensity I_0. As C is deposited during exposure in a hydrocarbon environment, the surface will grow though this standing wave resulting in large changes in the effective intensity. If the primary mechanism for C growth

were direct photon reactions with the adsorbed hydrocarbons, then this would clearly lead to a changing damage rate throughout the exposure as was observed in the previous section. It is more widely held, however, low-energy secondary electrons play the dominant role in C deposition [3,6,7] Even in this case, a similar variation in damage rate would be expected because the escape depth for the electrons is ~1 nm.[7,8] So the effective electron flux from the surface is determined by the value of the intensity over the first few nanometers below the surface.

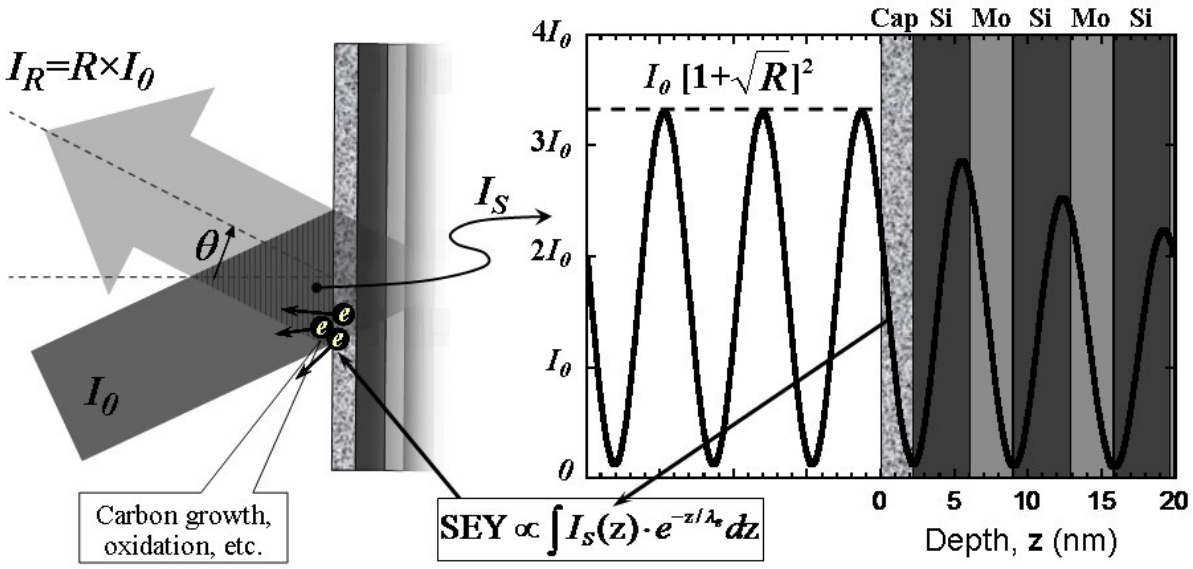

Fig. 3 The intensity interference pattern at the surface of a Ru-capped MLM is plotted in units of the incident intensity. The amplitude of the intensity standing wave in the vacuum is $I_0(1+\sqrt{R})^2$ which is approximately $3.4I_0$ corresponding to the $R = 0.66$ of the Ru-capped mirrors discussed here. As demonstrated on Si-capped MLMs the secondary electron yield (SEY) is determined by the field intensity in the first few nanometers below the surface. [7,8] The reaction rates for oxidation and carbon-growth should depend strongly on the SEY since both processes are driven by low-energy photoelectrons.[3]

To study this effect directly, a series of identical TiO_2 capped MLMs were fabricated at the IOF each with a different thickness of directly-deposited C on top. The thickness of this C layer would place the surface at different locations within the standing wave resulting in different electric field intensity at the surface. The secondary electron yields (SEY) of these samples were measured as a function of photon energy at normal incidence. The experiments were done under ultrahigh vacuum (UHV) conditions at beamline U3C (bending magnet) of NSLS at Brookhaven National Laboratory. Absolute values of SEY are based on measurements using a calibrated AXUV-100 silicon photodiode. Precision within a single set of measurements is estimated to be ± 5-10%, with absolute accuracy about twice that value. The details are reported elsewhere.[9]

As an example Figure 8 shows the experimental SEY data (filled circles) for the TiO_2-terminated MLM with no deposited carbon. All the measured SEY curves exhibited an interference structure (a phase effect) that differs dramatically for various carbon layer thicknesses (not shown). This phase effect in SEY of Si-terminated MoSi MLM was earlier reported by Underwood and Gullikson.[10] We have simulated this data using a model with several simplifying assumptions. The generation of photo electrons is described in our model by the total atomic photoionization cross section $\mu_i(h\nu)$ for each element i which is tabulated elsewhere.[11] The electron current density produced by atomic species i at the depth z is proportional to the number density of atom i and the photon intensity at that depth, $I_S(h\nu,z)$. For the atom i the number density is given by the ratio of the mass density $\rho_i(z)$ to the atomic mass $M_i(z)$ of the individual atom. The probability that an electron generated at depth z will make it to the surface is given by the exponential term $\exp(-z/\lambda(z))$ where $\lambda(z)$ is electron escape depth which we assumed to be 2× longer than the inelastic mean free path (IMFP) for 50 eV electrons; the IMFP values were taken from NIST database.[12] The assumption is based on earlier discussion of depth of origin of secondary electrons.[7,8] The third simplifying assumption is that the transport of

electron with various energies through vacuum/TiO_2 and vacuum/C interfaces is identical and, thus, the penetration of electrons through solid/vacuum barrier has a constant probability. This results in the following equation describing SEY as a function of photon energy:

$$SEY(h\nu) \propto \int_{\infty}^{0} \sum_i I_S(h\nu, z) \frac{\rho_i(z)}{M_i(z)} \mu_i(h\nu, z) e^{-z/\lambda(z)} dz \quad (1)$$

In this equation $I_S(h\nu,z)$ describes the distribution of photon intensity as a function of depth, z, below the surface and incident photon energy $h\nu$ calculated using IMD software.[13]

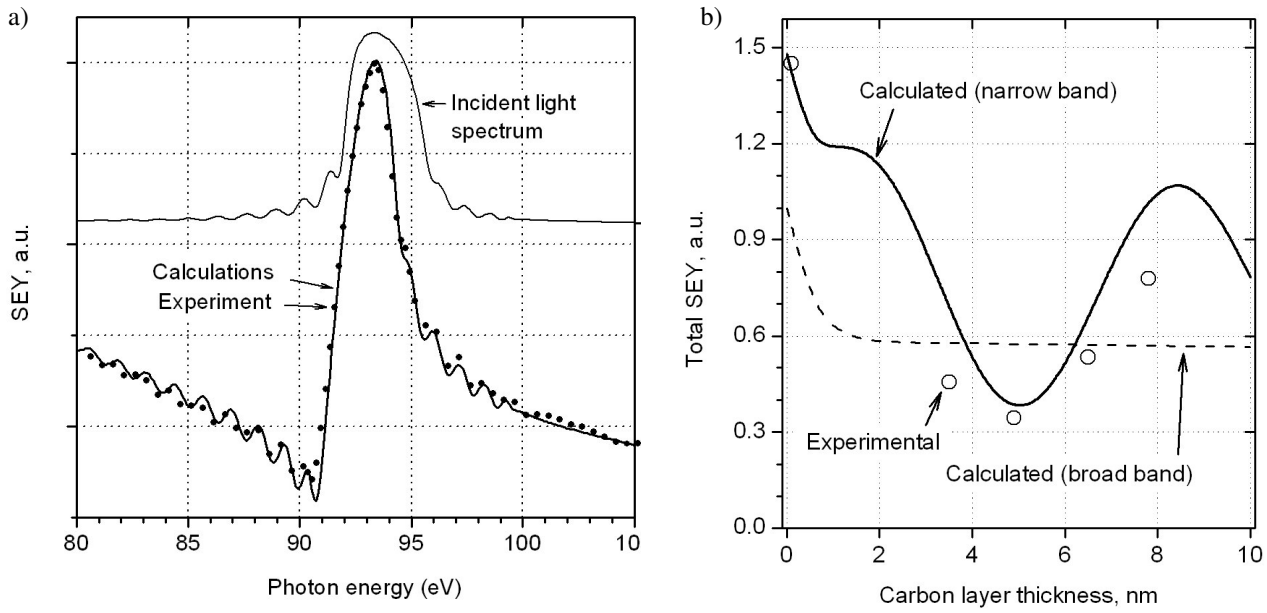

Fig. 8 (a) Experimental (dots) and calculated (thick solid line) SEYs as a function of photon energy in the vicinity of the resonance energy of MLM. The calculated values are the result of equation (1) and the known structure of the TiO_2-terminated MLMs produced at IOF. The thin line illustrates spectral function, $S(h\nu)$, of the EUV light to which MLMs in the NIST testing facility are exposed. (b) Total SEY as defined by equation (2) gives effective secondary electron flux at the surface by integrating the SEY($h\nu$) over the incident light spectrum. The measured SEY($h\nu$) for each sample were used to generate the "Experimental" open circles. The lines were generated using the calculated SEY($h\nu$) as a function of C thickness. In the case of broadband (dash line) incident light I_S=const and S=const; in the case of in-band (solid line) light I_S=$I_S(h\nu,z)$ and S($h\nu$) is from (a). Note that the Total SEY has been normalized to the broadband value with no C overlayer.

The thick solid line in Figure 8(a) shows the results of calculations. The best fit requires inclusion of about 2 monolayers of carbon on top of the cap, which is slightly thicker layer than one would expect for TiO_2 surface exposed to the air. Overall, the simulated curve reproduces the experimental results in the energy region which is close to the resonance reflection condition. Under realistic conditions, i.e. during EUV exposure either in a tool or in our test chamber, the emitted electron spectrum SEY($h\nu$) of MLM is modulated by the spectral function $S(h\nu)$ of incident EUV light. We estimated the Total SEY by integrating the product of the calculated SEY(hν) from equation (1) and the EUV spectral function $S(h\nu)$ over the measured photon energy range as shown by equation (2):

$$Total\ SEY \propto \int S(h\nu) SEY(h\nu) d\nu \quad (2)$$

For the case of exposures in our testing facility the spectrum of the incident light $S(h\nu)$ is determined by convolution of the measured reflectivity spectrum of the collector mirror and the known transmission of the Be filter. The EUV light spectrum corresponding to our conditions is shown by thin solid line in Figure 8(a). We used this spectrum in equation (2) to calculate the Total SEY as a function of carbon overlayer thickness. Figure 8(b) shows the experimental data (open circles) and calculated (solid line) values for the Total SEY(hν). The data are normalized to the value calculated for zero carbon thickness and broadband irradiation. There is good qualitative agreement between the solid calculated Total SEY and the measured values. These results demonstrate that the Total SEY can vary by more than a factor of 3 over several nm of C growth during resonant, in-band irradiation of a MLM. The calculated Total SEY for broadband illumination is also shown in Figure 8(b) (dashed curve). Note that this curve only displays the initial change in the SEY over the first 1-2 nm due to the difference in the photoemission between TiO_2 and C.

Since the Total SEY represents the effective secondary electron flux at the surface capable of reacting with adsorbed contaminant molecules, these results suggests that: (1) the damage rate for in-band irradiation could vary significant as the contaminant layer grows, as suggested by the MMA and acetone data shown in Figures 5 and 6; and (2) that the damage rates for broadband and in-band exposures could be very different. Note, however, that the exact shape of the resonant Total SEY curve in Figure 8(b) is determined entirely by the particular MLM structure, bandwidth and angle of incidence of irradiation used here. The shape of this curve for a different MLM irradiated under a different geometry could be quite different. The key point is that the damage rate could potentially depend critically on all these factors.

6. SUMMARY

The original approach to accelerated testing was based on learning how to correlate significant, measureable damage created by relatively short exposures under accelerated conditions of intensity and pressure with the much smaller damage rates induced under less harsh tool conditions over much longer periods of time. Our earlier accelerated testing experiments focused on photo-induced reaction of adsorbed water on Ru-capped MLMs and showed that the rate of reflectivity loss was a very complicated function of dose at high partial pressures of water.[14] These tests also indicated that ambient hydrocarbon species present at much lower concentrations than the admitted water were playing a key role.

The present work focuses on accelerated testing in which the predominant contaminant in the ambient vacuum is a hydrocarbon, either acetone or MMA. Here we have shown several important and somewhat unexpected results:

a) The rate of reflectivity loss can saturate at high partial pressure of the admitted hydrocarbon so that the damage does not scale with increasing pressure beyond a critical saturation pressure. The value of this critical pressure can vary widely for different gases. So accelerated testing by increasing the pressure of a particular gas should not be attempted until this saturation value is determined, and then only pressures below this value should be used.

b) The rate of reflectivity loss appears to change with dose during accelerated exposures for all the partial pressures investigated. The origin of these changes must be understood to extrapolate the low-dose damage rates relevant to the tool environment from the high-dose accelerated testing results.

c) A standing wave of EUV intensity is present at the surface of any MLM operating under resonant conditions. SEY measurements presented here also demonstrate a significant variation in the effective low-energy secondary electron flux at the surface. So whether the primary damage mechanism involves direct-photon interactions or low-energy secondary electrons, this implies that the damage rate could vary substantially as the thickness of the contamination layer increases and the surface moves through this varying light field. This is in agreement with the observed variation in damage rates discussed in b).

All of these results point to the fact that one must very carefully determine the circumstances under which one can extrapolate true rates of reflectivity loss under real operating conditions from tests under accelerated conditions.

ACKNOWLEDGEMENTS

All the authors would like to acknowledge the generous support of Intel Corporation. NIST authors would also like to thank Eric Gullikson and the staff at the ALS at LBL for thorough and timely reflectometry.

REFERENCES

[1] Silverman, P.J., "Extreme ultraviolet lithography: overview and development status", J. Microlith., Microfab., and Microsys. 4(1), 01100 (2005)

[2] Seisyan, R.P., "Extreme ultraviolet nanolithography for ULSI: A review", Techn. Phys. 50(5), 535-545 (2005)

[3] Madey, T.E., Faradzhev, N.S., Yakshinskiy, B.V., Edwards, N.V., "Surface phenomena related to mirror degradation in extreme ultraviolet (EUV) lithography", Appl. Surf. Sci. 253, 1691-1708 (2006)

[4] Faradzhev N.S., Kostov K.L., Feulner P., Madey T.E., Menzel D., "Stability of water monolayers on Ru(0001): thermal and electronically induced dissociation", Chem. Phys. Lett. 415, 165-171 (2005)

[5] Yakshinskiy, B., Hedhili, M. N., Chandhok, M., Madey, T.E., "Radiation-induced defect formation and reactivity on model TiO_2 capping layers with MMA", 2007 International EUVL Symposium, CC-P07, 28-31 October 2007, Sapporo, Japan

[6] Wasielewski, R., Yakshinskiy, B.V.; Hedhili, M. N., A. Ciszewski; Madey, T.E., "Surface chemistry of Ru: relevance to optics lifetime in EUVL", Proc. SPIE 6533, 653316 (2007)

[7] Hollenshead, J. and Klebanoff, L., "Modeling radiation-induced carbon contamination of extreme ultraviolet optics", J. Vac. Sci. Technol. B 24, 64-82 (2006).

[8] Yakshinskiy, B.V., Wasielewski, R., Loginova, E., Madey, T.E., "Carbon accumulation and mitigation processes, and secondary electron yields of ruthenium surfaces", Proc. SPIE 6517, 65172Z (2007)

[9] Yakshinskiy, B. V., Wasielewski, R., Loginova, E., Hedhili, M. N. Madey, T.E., "DIET processes on ruthenium surfaces related to extreme ultraviolet lithography (EUVL)", Surface Science (2008), in press

[10] Underwood, J.H. and Gullikson, E.M., "Beamline for measurement and characterization of multilayer optics for EUV lithography", Proc. SPIE 3331, 52-61 (1998)

[11] Dermott E. Cullen, John H. Hubbell, Lynn Kissel, "Evaluated photon data library, EPDL97", http://www-nds.iaea.org/epdl97/ (1997)

[12] Powell, C. J. and Jablonski, A., "NIST Electron Inelastic-Mean-Free-Path Database - Version 1.1", National Institute of Standards and Technology, Gaithersburg, MD (2000).

[13] Windt, D.L., "IMD--Software for modeling the optical properties of multilayer films", Computers in Physics 12 (4), 360-370 (1998)

[14] Hill, S.B., Ermanoski, I., Tarrio, C., Lucatorto, T.B., Madey, T.E., Chandhok, M., Fang, M., "Critical parameters influencing the EUV-induced damage of Ru-capped multilayer mirrors", Proc. SPIE 6517, 15 (2007)